To be submitted to
Nuclear Instruments
and Methods

ISTITUTO NAZIONALE DI FISICA NUCLEARE
Laboratori Nazionali di Frascati

LNF-82/14(P)
1 Marzo 1982

V. Bellini, E. De Sanctis, P. Di Giacomo, S. Gentile, C. Guaraldo, S. Lo Nigro, V. Lucherini, G. S. Pappalardo, E. Polli and A. R. Reolon: ON FISSION EXPERIMENTS BY MEANS OF A QUASI-MONOCHROMATIC PHOTON BEAM AT THE FRASCATI LINAC.

Servizio Documentazione
dei Laboratori Nazionali di Frascati
Cas. Postale 13 - Frascati (Roma)

INFN - Laboratori Nazionali di Frascati
Servizio Documentazione

LNF-82/14(P)
1 Marzo 1982

ON FISSION EXPERIMENTS BY MEANS OF A QUASI-MONOCHROMATIC PHOTON BEAM AT THE FRASCATI LINAC

E. De Sanctis, P. Di Giacomo, S. Gentile, C. Guaraldo, V. Lucherini, E. Polli, A. R. Reolon
INFN - Laboratori Nazionali di Frascati

V. Bellini, S. Lo Nigro and G. S. Pappalardo
Istituto di Fisica dell'Università di Catania, and INFN - Sezione di Catania

ABSTRACT.

The best experimental conditions to perform photofission measurements in the energy range 100 ÷ 300 MeV by using the Frascati annihilation photon beam are deduced. For nuclei with very low fission threshold energies it is shown to be advantageous to collect the photon beam at an angle $\vartheta_\gamma > 1^\circ$. For nuclei with high fission threshold energies, the annihilation photon contribution to the yield already predominates for $0.5^\circ \leq \vartheta_\gamma \leq 1^\circ$.

1. - INTRODUCTION.

The best tool to investigate photon induced nuclear reactions is represented by a monochromatic photon beam, since the experimental yields measured at different energies of the photon peak directly give the photoreaction cross section.

Unfortunately, the lack of a suitable powerful monochromatic gamma source, with continuously variable energy, gives rise to a strong constraint. At present, only "quasi monochromatic" photon beams can be produced by various techniques[1]. However, the characteristics of these photon sources often limit the kind of photonuclear experiments that one wants to carry on.

In this paper the advantage of using the quasi-monochromatic photon beam from annihilation in flight of positrons of the Frascati linac[2], in order to perform photofission measu-

rements, is analysed. This photon beam exhibits a monoenergetic peak at the correct annihilation energy, with a bremsstrahlung continuous tail. The energy of the peak can be continuously varied from 100 MeV up to 300 MeV. An accurate knowledge of photofission cross section in the above energy region can allow to deduce informations on photon-nucleus interaction in a region where the role of correlated neutron-proton pairs (quasi-deuteron model) and that of single nucleons (photomesonic model) are relevant.

The main features of the Frascati photon source are reported in Section 2. In this Section the characteristics of a magnetic pair-spectrometer, which enables to measure on-line the photon energy spectrum, are also reported. In fact, the exact knowledge of the photon spectrum is required in order to estimate the photofission cross section with a good degree of reliability. The best experimental conditions to perform fission measurements by using an annihilation photon beam are analysed in Section 3.

2. - THE FRASCATI PHOTON BEAM.

The monochromatic gamma beam facility from the Frascati Linac (LEALE photon facility) has already been described in detail in ref. (2). In Fig. 1 the experimental set up of the end-station of the facility is shown. Positrons leave the beam pipe through an aluminium window, 0.06 mm thick, and annihilate on a liquid hydrogen target, 0.0118 radiation lengths thick. The hydrogen cell is a kapton cylinder, 105 mm long, 55 mm diameter (wall thickness 0.125 mm). The cell is contained in a vacuum steel tank, with a thin kapton entrance window to the beam, 0.12 mm thick. The cell can be remotely removed from the beam path, allowing the insertion of a beam profile monitor.

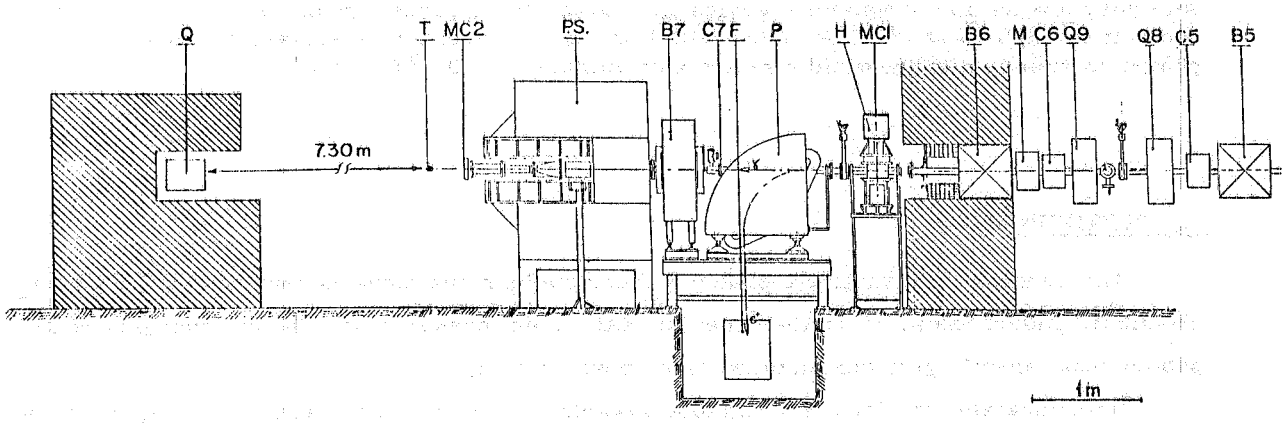

FIG. 1 - Layout of the positron-photon beam end-station: B5, B6 magnets; C5, C6 removable copper collimators (thickness 40 mm each, diameters 7 mm and 6 mm respectively); Q8, Q9 quadrupoles; M ferrite toroid monitor; MC1 positron beam profile monitor; H hydrogen target; P dumping magnet; F Faraday cup; C7 lead collimator; B7 sweeping magnet; PS pair spectrometer; MC2 photon beam profile monitor; T photoreaction target; Q quantameter.

The absolute value of the positron current is measured by a Faraday cup, put in the focal plane of a dumping magnet after the annihilation target. This magnet sweeps off from the photon beam the positrons which have not undergone annihilation. The intensity of the positron beam can also be continuously monitored by a non-intercepting ferrite toroid monitor, placed around the beam line, before the annihilation target.

The photon beam is defined by five cylindrical lead collimators (diameters: 9.0 mm, 10.0 mm, 10.5 mm, 11.5 mm, 12.2 mm respectively; 10.0 cm long each), inserted in the yoke of the dumping magnet and in the gap of the next sweeping magnet B7. The positron incidence angle on the annihilation target can be changed by two suitable bending magnets B5 and B6, which give two vertical deflections of opposite sign.

A rectangular flat pole (40×90 cm^2 size, 15 cm gap) C-type magnet is used as a pair spectrometer[3]. Photons enter the magnetic field region through a hole, 4 cm diameter, opened in the yoke of the magnet and hit one of the five available aluminium converters. Each converter is thin enough ($\leq 5 \times 10^{-4}$ radiation lengths) to minimize both beam attenuation and loss of efficiency due to multiple scattering and energy loss. In order to reduce background production from air, the beam channel, from the hydrogen target up to the spectrometer exit window is put under vacuum.

Electrons and positrons are deflected of about 110° by the spectrometer magnet, then leave the vacuum chamber passing through an aluminium window, 1 mm thick (see Fig. 2). The pairs detection is performed by two identical systems of plastic scintillators, each consisting of an array of four counters ($E_1, \ldots, E_4$ and $P_1, \ldots, P_4$), which are set along the focal line, followed by a fifth counter (E_5, P_5).

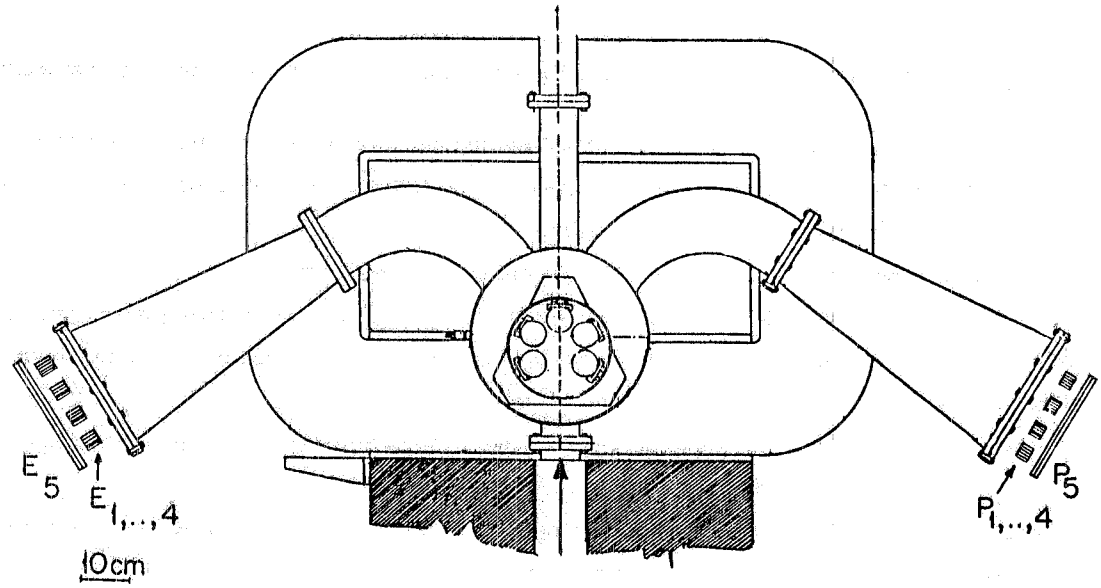

FIG. 2 - Pair spectrometer vacuum chamber with the associated electron (E_i) and positron (P_i) detection system.

In Fig. 3 the electronics block diagram is given: the E_i (P_i) discriminator outputs are sent to an OR circuit and then to a double coincidence with the fifth counter. Real and accidental coincidence signals enable the acquisition, via CAMAC, on a PDP 15/30 computer, of the signals from the counters of the two arms. Data analysis is performed on-line, allowing for a display of the photon spectrum on a storage oscilloscope.

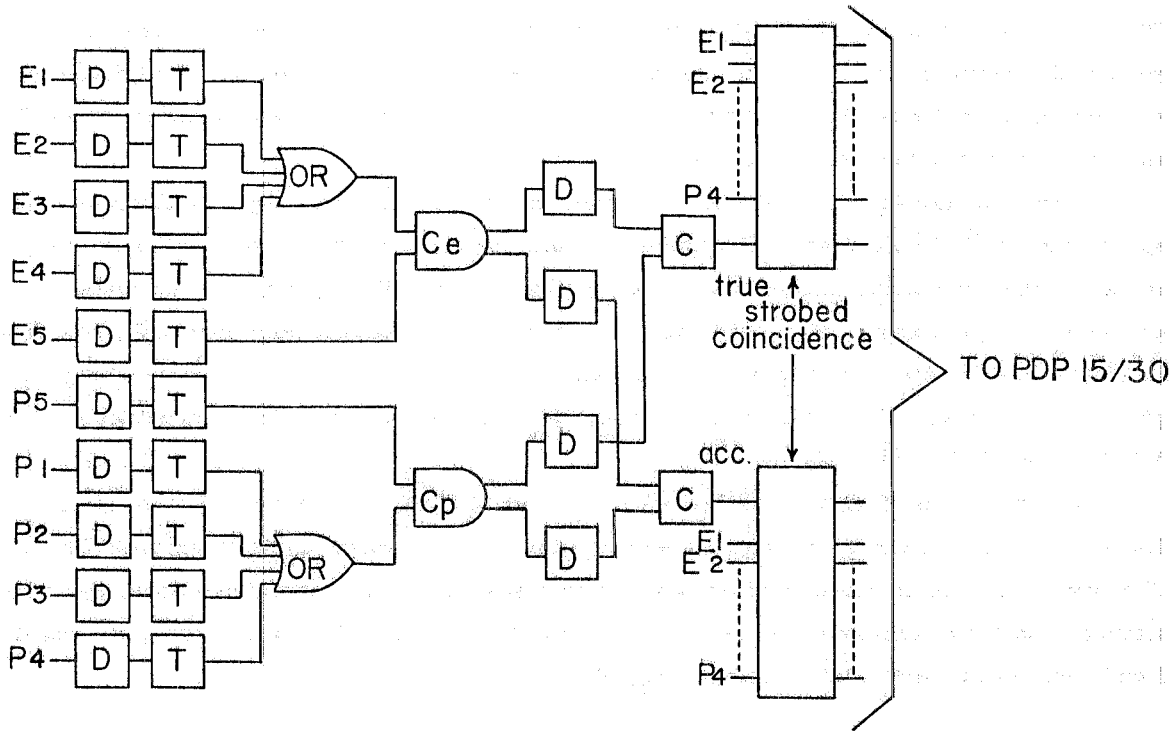

FIG. 3 - Electronics block diagram for the detection system of the pair spectrometer.

In Fig. 4 three typical energy spectra, measured at different positron energies E and photon collection angles ϑ_γ are shown. The full line curves have been obtained by a Monte Carlo simulation[4], which takes into account:

a) the positron beam characteristics (energy spread and emittance);
b) the different processes (annihilation, bremsstrahlung, multiple scattering and energy loss) undergone by positrons in all the materials (hydrogen target, alluminium and mylar windows, air) passed through along the beam path;
c) photon collection characteristics (diameter, thickness and relative position of the collimators).

As it can be seen in Fig. 4, the agreement between the data and the calculated curves is always satisfactorily within the experimental errors.

In Figs. 5, 6, 7 and 8 the photon features, as evaluated by the Monte Carlo calculation, are given. Inputs for the calculation have been the ordinary experimental conditions: i) posi

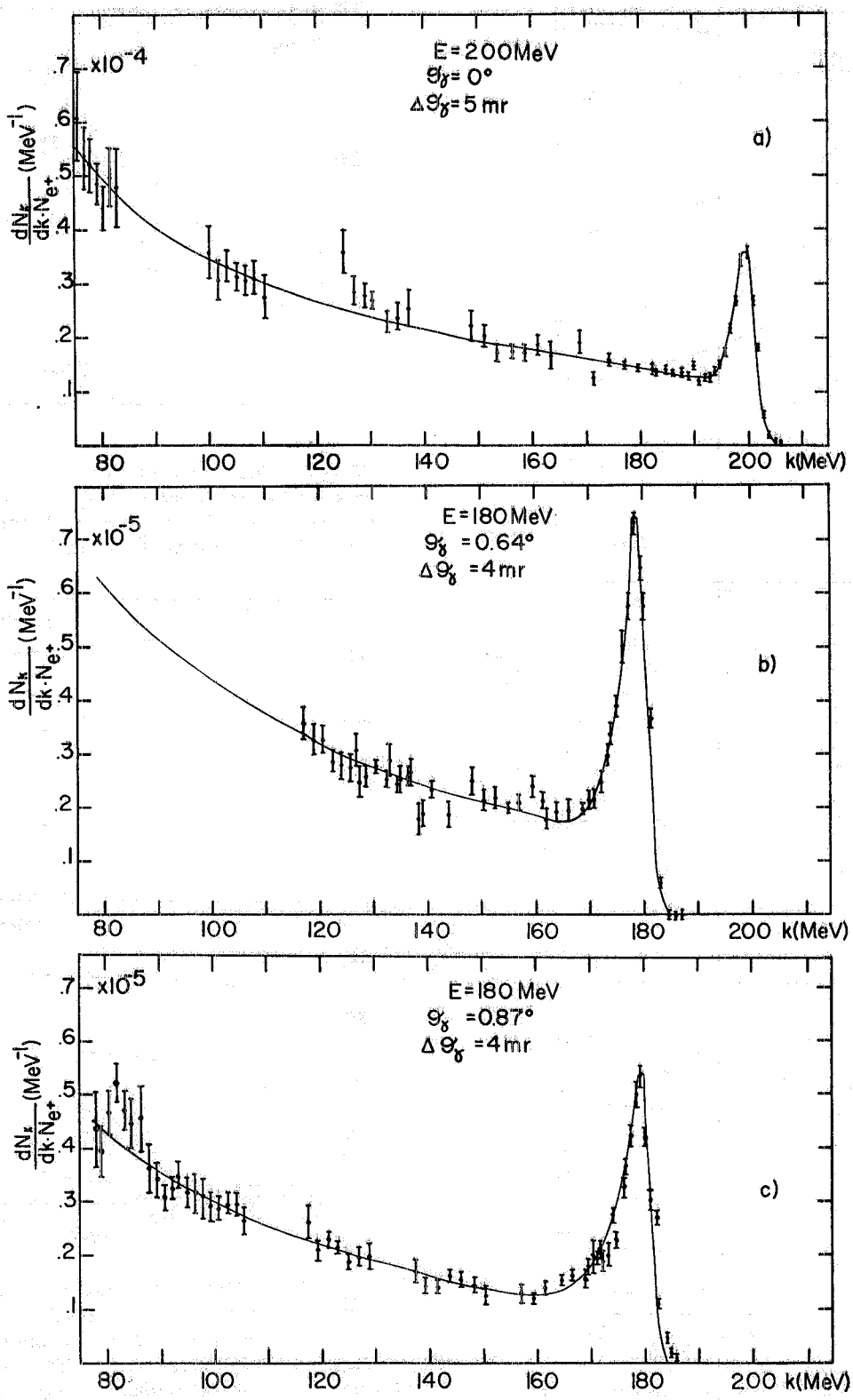

FIG. 4 - Photon energy spectra measured with the pair spectrometer at the given positron energies E, photon collection angles ϑ_γ and half angular geometric photon acceptances $\Delta\vartheta_\gamma$. The full lines spectra are calculated with a Monte Carlo program.

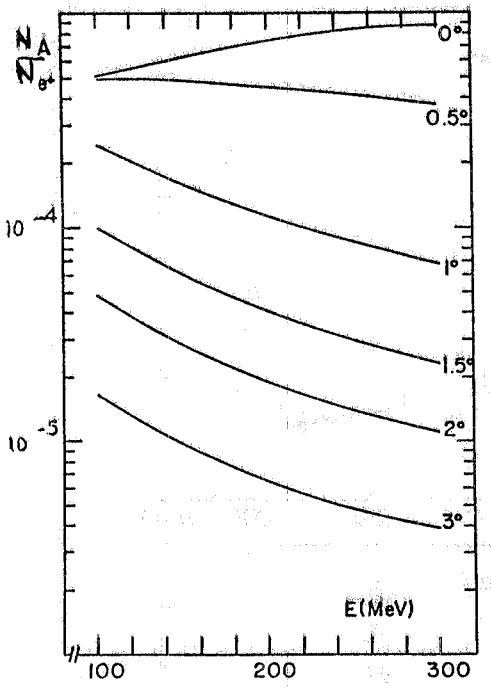

FIG. 5 - Monte Carlo calculation of the annihilation photon number per incident positron, N_A/N_{e+}, versus positron energy E, for different ϑ_γ values. Chosen calculation conditions: i) positron energy spread: 1.5% (FWHM); ii) positron emittance: radial 18 mm x mrad, vertical 15 mm x mrad; iii) liquid hydrogen annihilation target thickness: 105 mm; iv) photon geometric collection solid angle: 5.0×10^{-5} sr.

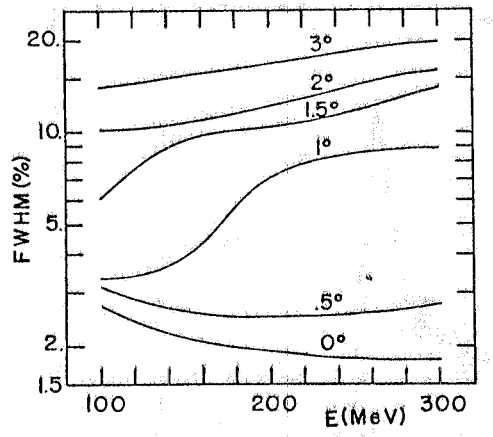

FIG. 6 - Monte Carlo calculation of annihilation photon peak FWHM (%) versus positron energy E, for various ϑ_γ values. Same conditions as in Fig. 5.

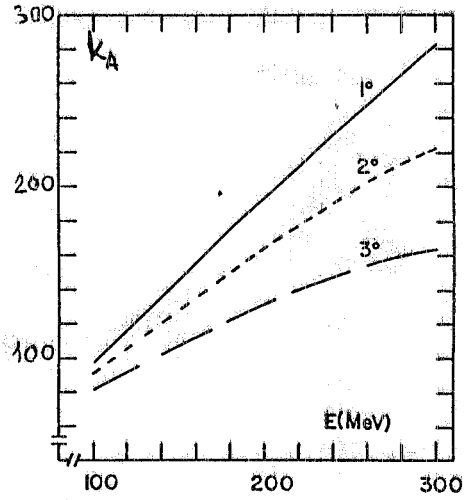

FIG. 7 - Monte Carlo calculation of annihilation photon peak energy k_A versus positron energy E for three different ϑ_γ values. Same conditions as in Fig. 5.

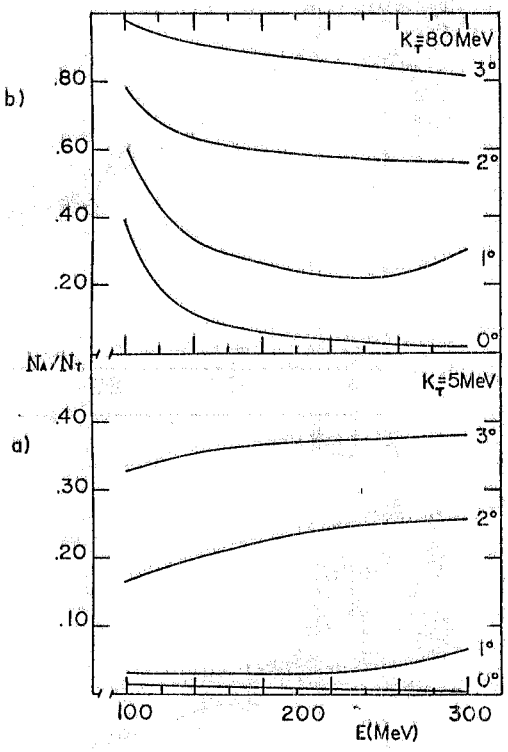

FIG. 8 - Monte Carlo calculation of the ratio between the number of annihilation photons N_A and the total number of photons N_T versus positron energy E for different ϑ_γ values. Low cut-off photon energy k_T: a) 5 MeV; b) 80 MeV. Same conditions as in Fig. 5.

tron energy spread 1.5%; ii) positron radial and vertical emittance 18 mm x mr and 15 mm x mr respectively; iii) photon collection geometric solid angle 5×10^{-2} msr.

In Fig. 5 the number of annihilation photons per incident positron N_A/N_{e+} is reported.

In Fig. 6 the full width half maximum of the annihilation peak, as a function of the positron energy, for various collection angles, is reported.

The annihilation photon peak energy, as a function of the positron energy, for different collection angles, is reported in Fig. 7. Because of the finite angular acceptance and of the positron energy loss in the target, the peak energy results slightly different from the pure kinematic value.

Finally, in Fig. 8 the behaviour of the ratio N_A/N_T versus the positron energy, for settled values of the photon collection angle, is given (N_T is the total number of photons in the spectrum whose energy is greater than a fixed threshold k_T). It is clearly seen that, by increasing the photon collection angle, the ratio improves. In the meanwhile, however, photon intensity strongly decreases and resolution gets worse, as Figs. 5 and 6 show.

3. - PHOTOFISSION MEASUREMENTS.

The use of a quasi-monochromatic photon beam from positron annihilation in photofission measurements, instead of a bremsstrahlung one, gives a remarkable improvement in data quality, if the contribution to the fission processes from the monochromatic peak is relevant compared to that from the bremsstrahlung tail. To this aim, the behaviour of the fission fragments yield, for an assumed photofission cross section and for given photon spectra, at different photon collection angles, has been evaluated.

The calculation has been performed for two different groups of nuclei:

a) nuclei with $Z \geq 90$, for which the fission energy threshold lies below the giant dipole resonance (GDR);

b) nuclei with $Z \leq 83$, for which the fission threshold is above the GDR, but below the pion photoproduction threshold.

The photofission yields $g(k_m)$ have been calculated by folding the integral equation of the process

$$g(k_m) = \int_{k_T}^{k_m} N(k, k_m)\, f(k)\, dk \qquad (1)$$

where $N(k, k_m)$ is the number of photons in the energy interval from k to $k+dk$; k_m is the maximum photon energy, assumed equal to the positron energy; k_T is the fission energy threshold and $f(k)$ is the photon fission cross section.

By means of the above mentioned Monte Carlo calculation, eleven photon spectra have been evaluated for positron energies from 100 MeV up to 300 MeV, with 20 MeV energy intervals, and for photon collection angles ranging from 0^o up to 2^o. The upper limit for ϑ_γ has

been chosen taking into account both the results reported in Figs. 5, 6 and 8 and the expected low photofission cross section in the considered energy range.

The integral (1) has been numerically solved by means of the Simpson formula.

3.1. - Nuclei with $Z \geq 90$.

In the case of nuclei with $Z \geq 90$, due to the low fission energy threshold, a large contribution to the yield comes from the absorption of photons with energy in the GDR region.

The calculation has been performed for the ^{238}U nucleus, for which the photofission cross section f(k) is known in literature. The chosen function f(k) is reported in Fig. 9. In the figure, the dashed curve is the behaviour, as deduced from the results of various authors[5,6], up to 100 MeV; continuous one represents the behaviour obtained from measurements by a coherent photon beam at the Frascati synchrotron[7].

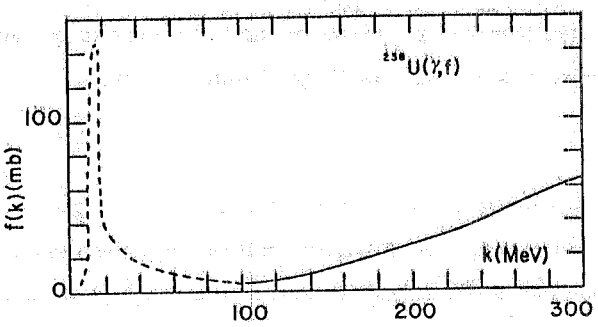

FIG. 9 - Absolute photofission cross section f(k) for ^{238}U versus photon energy k. The values are deduced from refs. (5, 6) (dashed curve) and from ref. (7) (solid curve).

The yields $g(k_m)$ deduced at different collection angles are reported in Fig. 10, as a function of the maximum photon energy (continuous curves). In the same figure, the dashed curves represent the yields $g_B(k_m)$ obtained by considering only the bremsstrahlung photons. For $\vartheta_\gamma = 0°$ the two curves coincide within the used scale.

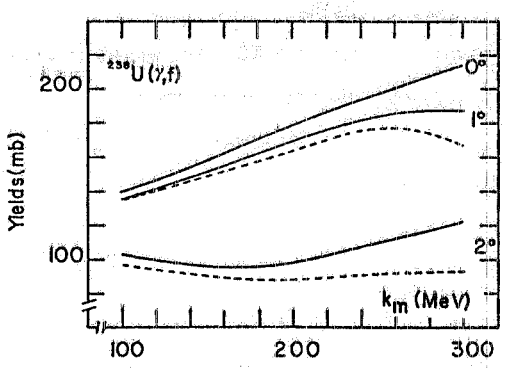

FIG. 10 - Absolute photofission yields per equivalent quantum $g(k_m)$ for ^{238}U versus maximum photon energy k_m at three photon collection angles ϑ_γ (continuous curves). The dashed lines represent the calculated yields $g_B(k_m)$ from the absorption of bremsstrahlung photons. At $\vartheta_\gamma = 0°$ continuous and dashed lines are coincident within the used scale.

In Fig. 11 the ratio $[g(k_m) - g_B(k_m)]/g(k_m)$ is reported. It represents the contribution to the yield from the annihilation photons compared to that from the whole spectrum. This contribution for $\vartheta_\gamma = 0°$ is very small, so that, as previously said, the annihilation + bremsstrahlung yield turn out to be very like to the bremsstrahlung one.

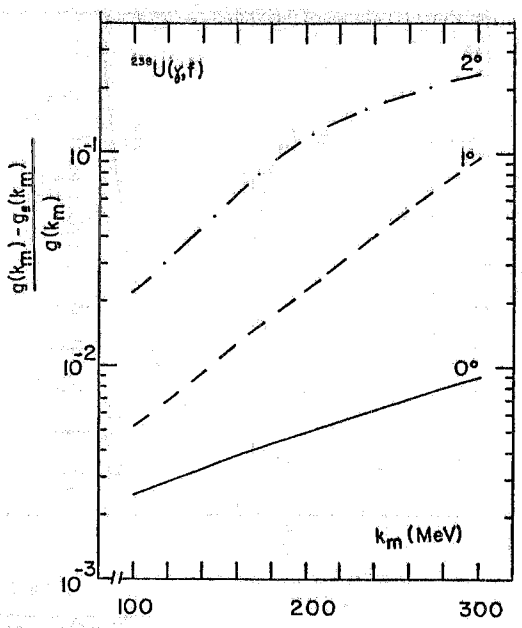

FIG. 11 - Annihilation peak relative contribution to the total yield for ^{238}U.

3.2. - Nuclei with $Z \leq 83$.

In the case of nuclei with $Z \leq 83$, the contribution to fission processes of the absorption of photons in the GDR region is negligible, because of the high fission energy threshold.

The calculation has been performed for Bi and Au nuclei, by assuming for the cross section the behaviour obtained in previous measurements[8] and reported in Fig. 12. Moreover, because of the low photofission cross section at energies less than 80 MeV, in folding eq. (1) we have taken k_T = 80 MeV.

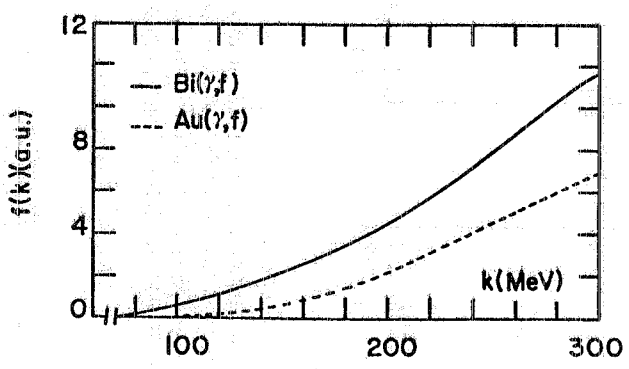

FIG. 12 - Photofission cross section f(k) (a.u.) versus photon energy k. Continuous curve: Bi; dashed curve: Au (deduced from ref. (8)).

The fission yields obtained at 0°, 1°, 2° photon collection angles are shown in Fig. 13. It is again noteworthy the advantage, compared to a bremsstrahlung beam, one gets from a non-forward collection angle. This can be seen more clearly in Fig. 14, where the ratio $[g(k_m) - g_B(k_m)]/g(k_m)$ is reported.

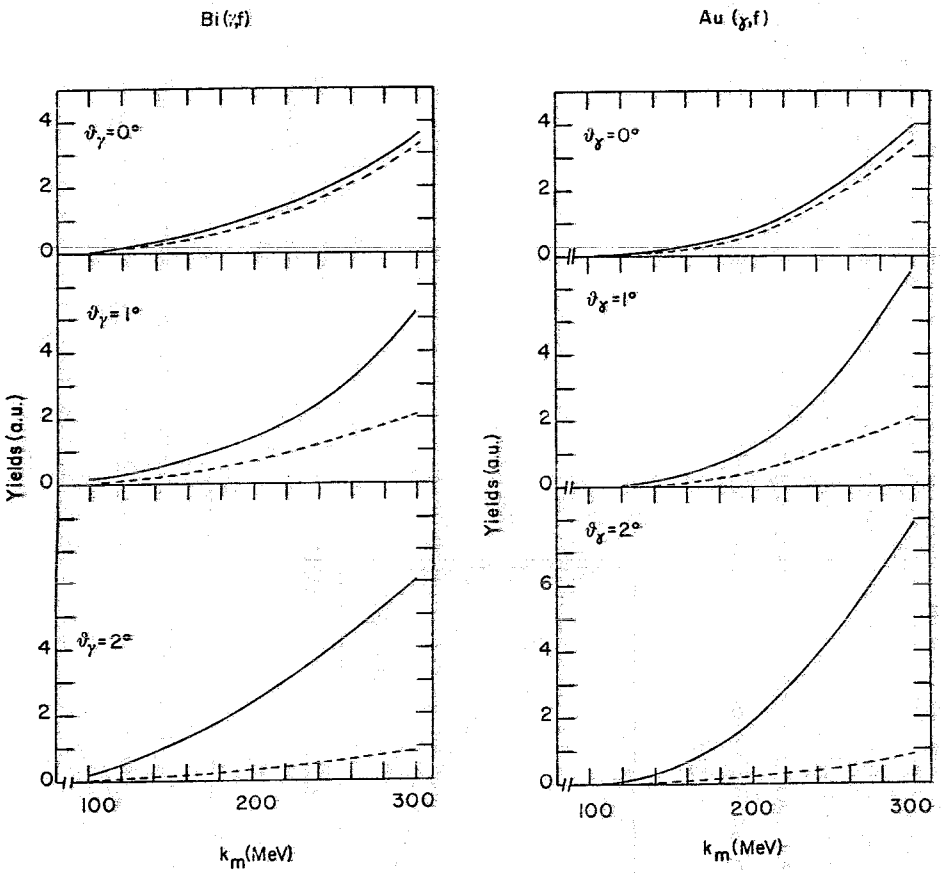

FIG. 13 - Photofission yields per equivalent quantum $g(k_m)$, for Bi (a) and Au (b), versus k_m at three photon angles ϑ_γ (continuos curves). The dashed lines represent the calculated yields $g_B(k_m)$ from the absorption of the bremsstrahlung part of the photon spectrum.

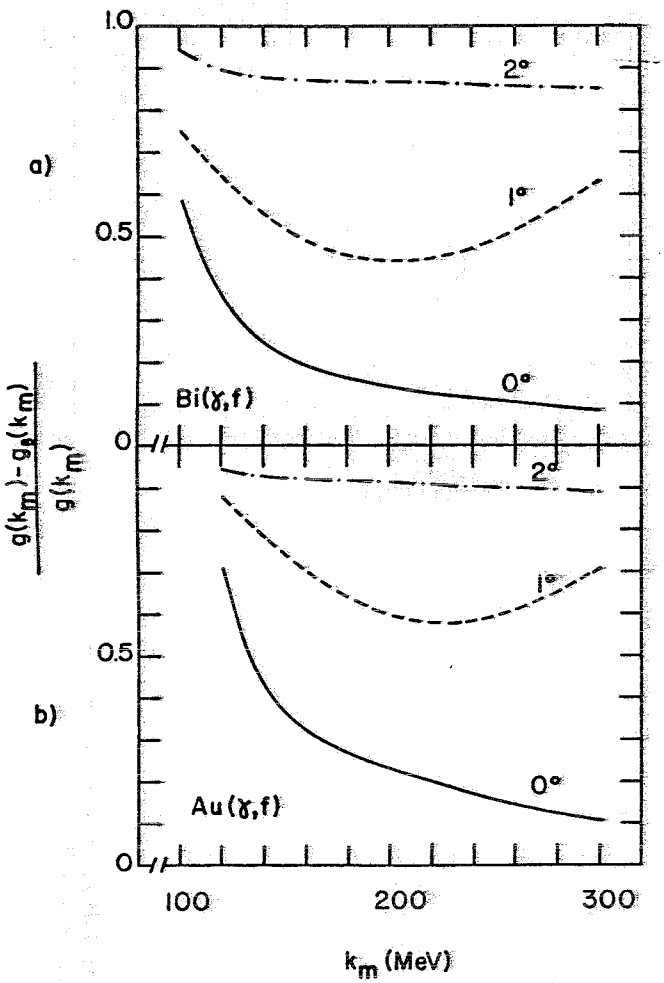

FIG. 14 - Annihilation peak relative contribution to the total yield for Bi (a) and Au (b).

4. - CONCLUSIONS.

In Fig. 15 the relative contribution to the fission yield from the annihilation photon peak, is given, for different positron energies, as a function of the photon collection angle. Figs. 15 a) and b) refer to nuclei with low and high fission threshold energies, respectively. For the sake of convenience, in Fig. 15c) the number of annihilation photon per incident positron, for the same values of ϑ_γ and E, is reported.

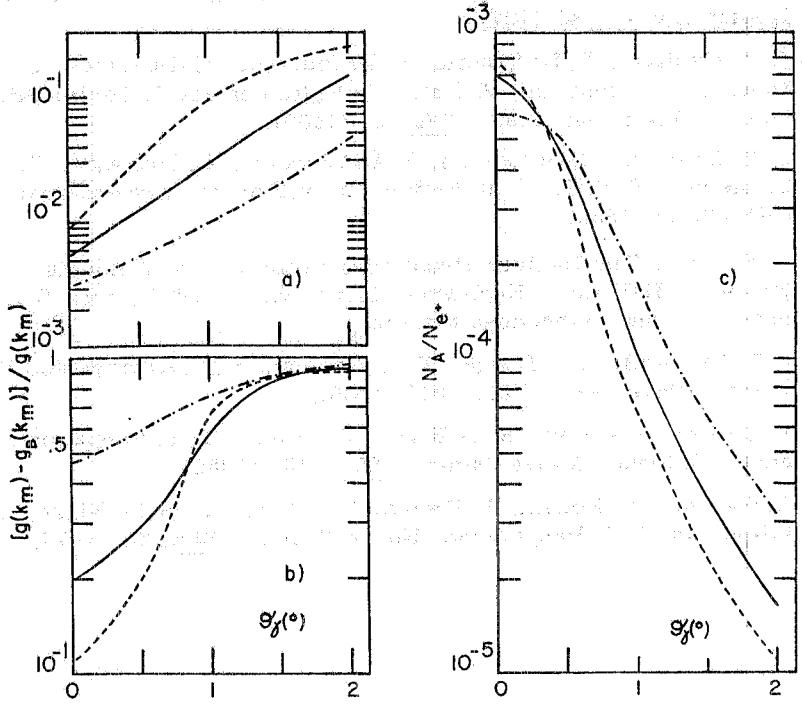

FIG. 15 - Annihilation peak relative contribution to the total yield estimated for ^{238}U (a) and Au (b) as a function of the photon collection angle. In c) the annihilation photon number per incident positron is given. Dot-dashed line positron energy E = 140 MeV, full line E = 220 MeV, dashed line E = 300 MeV.

From the figure it can be deduced that a remarkable advantage is achieved by using an annihilation photon beam at collection angles as higher as possible, taken into account that the annihilation intensity strongly decreases with increasing ϑ_γ. Namely, for nuclei with low fission threshold energy, the high fission cross section enables to use annihilation beam at $\vartheta_\gamma > 1^\circ$, in spite of the low photon intensity. On the contrary, the low fission cross section for $Z \leq 83$ nuclei advises against the use of collection angles $\vartheta_\gamma > 1^\circ$. However in this case, due to the high fission threshold energy, the annihilation peak contribution to the yield already predominates for $0.5^\circ \leq \vartheta_\gamma \leq 1^\circ$.

REFERENCES.

(1) - H. Beil and R. Bergère, Report CEA-N-2144 (1980).

(2) - G. P. Capitani, E. De Sanctis, P. Di Giacomo, C. Guaraldo, G. Ricco, M. Sanzone, R. Scrimaglio and A. Zucchiatti, Proceedings Few Body Systems and Electromagnetic Interactions, Ed. by C. Ciofi degli Atti and E. De Sanctis, Lectures Notes in Physics (Springer Verlag, Berlin, 1977), vol. 86, pag. 127; Frascati Report LNF-77/45 (1977).

(3) - G. P. Capitani, E. De Sanctis, P. Di Giacomo, C. Guaraldo, S. Gentile, V. Lucherini, E. Polli, A. R. Reolon and R. Scrimaglio, Nuclear Instr. and Meth. 178, 61 (1980).

(4) - G. P. Capitani, E. De Sanctis, P. Di Giacomo, C. Guaraldo, V. Lucherini, E. Polli, A. R. Reolon and V. Bellini, Frascati report LNF-82/12 (1982).

(5) - E. K. Hyde, The Nuclear Properties of the Heavy Elements (Prentice Hall Inc., Englewood Cliffs, N. J., 1964), vol. III, chap. 13, and references therein.

(6) - J. T. Caldwell, E. J. Dowdy, B. L. Berman, R. A. Alvarez and P. Meyer, Phys. Rev. C21, 1215 (1980).

(7) - V. Bellini, V. Emma, S. Lo Nigro, C. Milone, G. S. Pappalardo and G. Bologna, Nuovo Cimento 55A, 182 (1980).

(8) - G. Bologna, V. Bellini, V. Emma, A. S. Figuera, S. Lo Nigro, C. Milone and G. S. Pappalardo, Nuovo Cimento 35A, 91 (1976).